ELSEVIER

Advances in Water Resources 25 (2002) 591–599

Advances in Water Resources

www.elsevier.com/locate/advwatres

Frozen barrier evolution in saturated porous media

A.Y. Sheshukov [a,*], A.G. Egorov [b]

[a] Department of Biosystems and Agricultural Engineering and Army High Performance Computing Research Center, University of Minnesota, 1390 Eckles Avenue, Saint Paul, MN 55108, USA

[b] Chebotarev Research Institute of Mathematics and Mechanics, Kazan State University, 17 Universitetskaya Street, Kazan 420008, Russia

Received 26 March 2001; received in revised form 8 March 2002; accepted 14 April 2002

Abstract

A numerical model capable of simulating the freezing of aqueous solution flow in saturated porous media is presented. This model is based on a finite-difference approximation of the coupled equations for liquid water flow, heat and solute transport and phase change. The phase change equation facilitates the condition for the special case when liquid water and ice can reside in the pore space simultaneously, leading to a 'mushy' zone. Results are presented to show the evolution of multiple frozen regions growing by a chain of freezing pipes. Two different regimes for the evolution of frozen bodies are distinguished based on system parameters. For the regime with lower freezing rate separate frozen bodies exist at steady-state, while for higher freezing rate the regime is characterized by linked frozen bodies. The numerical solution for the first regime is tested by a semi-analytical solution for the case of fresh water. For the second regime the model is able to simulate the process up to the point when linking of the separate frozen bodies occurs. For both regimes freezing is hindered downgradient of the freeze pipe where solute becomes highly concentrated, and a wedge of unfrozen media forms. For the first regime the wedge eventually forms into a liquid 'island' surrounded by ice-bearing porous media.

Keywords: Soil freezing; Frozen barrier; Mushy zone; Numerical modeling

1. Introduction

The freezing of saturated geological material is a technology that can be applied beneficially to solve problems faced in groundwater contaminant remediation and in construction activities. One particular application involves the isolation of a saturated region from the main groundwater flow by using a series of vertical freezing pipes to produce a line of linked frozen bodies essentially impermeable to groundwater flow [1,2]. Prediction of the process of frozen barrier formation and the design of mechanical/thermal systems to produce a frozen barrier involves the specification of equations for fluid flow, heat and solute transport, and phase change. These equations are rather complicated, therefore, most research efforts to date have studied the equations under simplifying assumptions.

The equilibrium shape of a frozen body grown by a freeze source in an air-free porous medium saturated by fresh water was studied by Goldstein and Reid [3] and in series of publications by Kornev et al. [4–6]. They formulated the problem by classical mathematical approach called here the *Stefan model*, and applied a complex variables technique to develop a semi-analytical solution.

The Stefan model is based on the presence of a sharp interface dividing the whole domain on two subdomains: the unfrozen ice-free and the fully frozen water-free region. It is known from the literature [7–10] that in reality there exists an interfacial zone, with ice and liquid being present in the pore void, sandwiched between the fully frozen region and the unfrozen region. This interfacial zone is produced by the variation in freezing temperature, such variation being due to capillary effects [8,11] or osmotic potential effects [10,12]. The osmotic potential effect is seen, for example, during the solidification of binary solutions [9,13,14]. A full model of freezing should incorporate the effects of both capillarity and osmotic potential, as both forces will have a significant

* Corresponding author.

E-mail addresses: shesh002@umn.edu (A.Y. Sheshukov), andrey.egorov@ksu.ru (A.G. Egorov).

0309-1708/02/$ - see front matter
PII: S0309-1708(02)00033-7

impact on different stages of the frozen barrier evolution and maintenance. In this paper, we focus only on the barrier *evolution* stage. This stage is viewed to be a short-term process accompanied by a high external thermal input to the saturated porous medium. In this situation, it seems reasonable to ignore prevalent mechanisms of capillarity and diffusion which are negligibly small in comparison with osmotic forces and fluid convection, respectively. This assumption should be valid for coarse-grained porous media with a strong groundwater flow. The contribution of capillarity and diffusion is apparently essential for the long-term maintenance of frozen barriers. However, a comprehensive analysis needs to be done to study the long-term behavior of a frozen barrier, and this is not within a scope of the present study.

In this paper, we will keep the nomenclature accepted in solidification theory and refer to the unfrozen region as the *liquid zone*, the fully frozen region as the *solid zone*, and the interfacial region as the *mushy zone*, taking into account the presence of the porous matrix in all regions. It is emphasized that we deal only with air-free porous media regardless of ice being present or not in pore voids.

In the liquid and solid regions the system of equations is well-known and may be written as in [15], while to study the macro-scale dynamics of the transport processes in the mushy zone, the amount of unfrozen liquid is quantified by a liquid fraction function based upon a condition of local thermodynamic equilibrium. Therefore, the mathematical model consists of the set of governing equations for mass of water, solute component, and energy as well as local thermodynamic equilibrium. It is very difficult to derive analytical solutions due to the presence of solute, so a numerical solution seems to be an appropriate tool to study the problem. The objectives of this paper are (1) to present the derivation of a numerical solution scheme capable of solving the problem without separating the domain a priori into liquid, solid and mushy subdomains and (2) to simulate saturated porous media freezing by a chain of freezing pipes to create a barrier to groundwater flow.

The paper is organized as the following. In Section 2, we formulate the mathematical model and write the system of equations equally suitable for the liquid, solid, and mushy zones. Discretization of the balance equations and the procedures for the numerical solution are presented in Section 3. In Section 4, numerical results for the case of solute-free water and for aqueous solutions are presented. A semi-analytical solution [6] is used as a point of comparison for these numerical solutions. General conclusions of the study are presented in Section 5.

2. Statement of problem

The physical system we study is shown in Fig. 1. We consider a two-dimensional system in which frozen

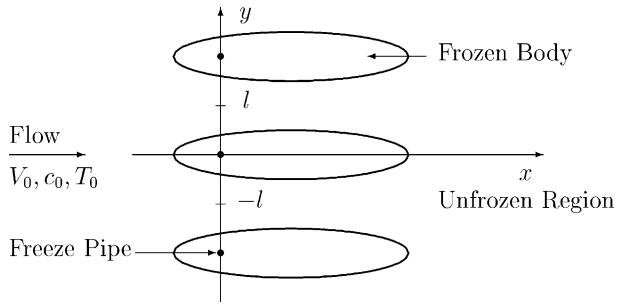

Fig. 1. Configuration of two-dimensional multiple frozen regions. Frozen bodies developed around the freeze sources (shown as bold dots) may eventually link and form a frozen barrier for liquid flow in the porous media.

volumes are developed by freeze pipes located in a horizontal field of uniform fluid flow. Freeze pipes with the freezing rate q form an infinite chain along the y-axis with a distance $2l$ between each adjacent pair. At infinite distance ($x \to -\infty$) upstream to the freeze pipe, the incoming liquid has the temperature T_0 and the concentration c_0, and moves with the velocity V_0 ($V_x = V_0$, $V_y = 0$). These boundary conditions also characterize the system at the initial time ($t = 0$).

The system of conservation equations for the aqueous solution, solute and heat may be written as [10,16,17]

$$\phi \frac{\partial}{\partial t}(\rho_w S + \rho_i(1-S)) + \rho_w \nabla \cdot \vec{V} = 0, \tag{1}$$

$$\vec{V} = -K \nabla p, \tag{2}$$

$$\phi \frac{\partial Sc}{\partial t} + \nabla \cdot (c\vec{V}) = \nabla \cdot (\phi S D \nabla c), \tag{3}$$

$$\frac{\partial}{\partial t}(CT + \rho_i \phi L S) + C_w \nabla \cdot \left(T\vec{V}\right) = \nabla \cdot (\lambda \nabla T). \tag{4}$$

In these equations, S is the saturation (degree of pore void filled by liquid), $\vec{V}$ is the liquid flux, p is the pressure head, c is the concentration of aqueous solution, T is the temperature, ϕ is the porosity, D is the diffusion coefficient, C is the heat capacity, λ is the thermal conductivity, L is the latent heat of freezing, ρ is the density, K is the hydraulic conductivity, and subscripts 'i' and 'w' indicate ice and liquid respectively. Note that $(1 - S)$ is the ice saturation, since the porous medium is air-free. Also note that hydrodynamic dispersion has been neglected in Eq. (3) because we assume the porous medium to be homogeneous at all length scales.

Darcy's law, given by (2), with the liquid fraction dependent hydraulic conductivity $K(S)$ is applied for fluid flow, as done in previous studies on freezing of saturated porous medium [10,11,17] as well as solidification of binary solutions [9,13]. The hydraulic conductivity function is given by $K(S) = K_0 S^n$, where K_0 is the saturated hydraulic conductivity and the exponent n is taken to be in the range $2 \leqslant n \leqslant 3$ [11]. Eq. (3) assumes

that all solute is rejected into the liquid during freezing, and ice always remains pure.

The four governing equations, (1)–(4), contain five unknowns S, $\vec{V}$, p, c and T. The model is completed by writing the condition of phase state distinguishing the type of the region: liquid zone, solid zone or mushy zone. For the first two types the condition is trivial. In fact, saturation is equal to unity for the liquid zone, while saturation is equal to zero for the solid zone. The mushy zone is assumed to be in local thermodynamic equilibrium so that the temperature relates to the concentration there by the following equation [12,13]:

$$\rho_w \frac{L}{T_f}(T - T_f) + \mathscr{R} T_f c = 0, \tag{5}$$

where $T_f = 273.15$ K is the freezing temperature of pure water, and $\mathscr{R}$ is the universal gas constant. Conditions defining the type of zone may be summarized via the following relationship illustrated in Fig. 2:

$$S \in \mathscr{H}(T - T_f + \gamma c), \tag{6}$$

where $\gamma = \mathscr{R} T_f^2/(\rho_w L)$ is known as the cryoscopic constant, and $\mathscr{H}$ is the Heaviside step-function multi-valued at $T = T_f - \gamma c$. Eq. (6) means that the liquid zone ($S = 1$) exists if $T > T_f - \gamma c$, the solid zone ($S = 0$) exists if $T < T_f - \gamma c$, and the equilibrium condition (5) is fulfilled within the mushy zone ($0 < S < 1$). In the mushy zone the saturation must be found as a solution to the system of equations (1)–(5). Eq. (6) is the general description incorporating all the zones, solid, liquid and mushy. Therefore, the set of Eqs. (1)–(4), along with (6) are suitable to describe all three zones.

Trying to keep the model as simple as possible, we make the following assumptions. We ignore the change in specific volume of water during phase transition. We neglect a diffusive mechanism of solute transport, which enables us to focus attention on the effects of forced convection as well as heat transfer. This approximation is valid if the Lewis number ($Le = \lambda/(CD)$) is much larger than unity, which is typical for liquids. For clarity of presentation, both the heat capacity C and the thermal conductivity λ are also assumed to be constant.

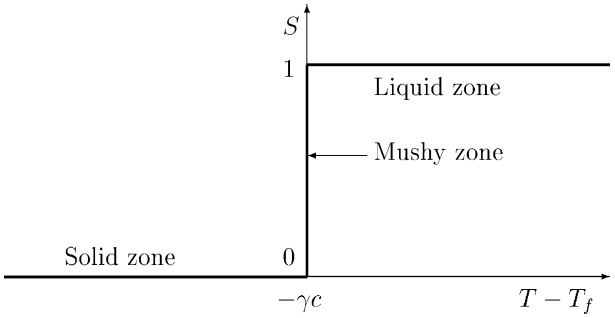

Fig. 2. Liquid saturation vs. temperature. Mushy zone occurs if $T - T_f = -\gamma c$.

Scaling unknowns with their reference values, we introduce the following non-dimensional variables (denoted by subscript 'u')

$$x_u = \frac{x}{l}, \quad y_u = \frac{y}{l}, \quad t_u = \frac{t\lambda}{Cl^2},$$

$$p_u = \frac{pK_0}{lV_0}, \quad \vec{V}_u = \frac{\vec{V}}{V_0}, \quad K_u = \frac{K}{K_0},$$

$$T_u = \frac{T - T_f}{T_0 - T_f + \gamma c_0}, \quad c_u = \frac{\gamma c}{T_0 - T_f + \gamma c_0},$$

$$q_u = \frac{ql}{\lambda(T_0 - T_f + \gamma c_0)}.$$

The non-dimensional form of the conservation equations (1)–(4) and (6) is as follows (we drop the subscript 'u' for convenience):

$$\nabla \cdot \vec{V} = 0, \tag{7}$$

$$\vec{V} = -K(S)\nabla p, \tag{8}$$

$$\phi_t \frac{\partial Sc}{\partial t} + Pe\nabla \cdot (c\vec{V}) = 0, \tag{9}$$

$$\frac{\partial T}{\partial t} + St\frac{\partial S}{\partial t} + Pe\nabla \cdot (T\vec{V}) = \Delta T, \tag{10}$$

$$S \in \mathscr{H}(T + c). \tag{11}$$

The non-dimensional parameters are the Peclet number, Pe, the Stefan number, St, and the thermal porosity, ϕ_t:

$$Pe = \frac{lC_w V_0}{\lambda}, \quad St = \frac{\rho_i \phi L}{C(T_0 - T_f + \gamma c)}, \quad \phi_t = \phi\frac{C_w}{C}.$$

For numerical calculations we consider the infinite horizontal layer, $-\infty < x < \infty$, $0 \leqslant y \leqslant 1$. The line $y = 1$ is the line of symmetry between two freeze sources, while the line $y = 0$ is the line of symmetry passing through the freeze source and the center of coordinates $x = 0, y = 0$. Then, the system of equations (7)–(11) with five unknowns $\vec{V}$, p, T, c, and S is complemented by the following initial and boundary conditions (δ is the Dirac function):

$$t = 0: \quad V_x = 1, \ V_y = 0, \ c = c_0, \ T = 1 - c_0, \tag{12}$$

$$x \to -\infty: \quad V_x = 1, \ T = 1 - c_0, \ c = c_0, \tag{13}$$

$$x \to \infty: \quad V_x = 1, \ \frac{\partial T}{\partial x} = 0, \tag{14}$$

$$y = 1: \quad V_y = 0, \ \frac{\partial T}{\partial y} = 0, \tag{15}$$

$$y = 0: \quad V_y = 0, \ \frac{\partial T}{\partial y} = -\frac{q}{2}\delta(x). \tag{16}$$

3. Numerical method

The system of governing equations (7)–(11) together with initial and boundary conditions (12)–(16) is solved numerically by applying a mesh-centered finite-difference method. For numerical simulation the infinite region is reduced to the domain $x_l \leqslant x \leqslant x_r$, $0 \leqslant y \leqslant 1$. We use the Cartesian grid (x_i, y_j) which is non-uniform in the both x and y directions with variable grid spacings $h_i^x = x_{i+1} - x_i$ and $h_j^y = y_{j+1} - y_j$ ($\hbar_i^x = 0.5(h_i^x + h_{i-1}^x)$ and $\hbar_j^y = 0.5(h_j^y + h_{j-1}^y)$). Grid spaces h_i^x and h_j^y are assumed to be a constant within the region $|x| < 1$, $0 \leqslant y \leqslant 0.05$, while outside this region they increase in geometric sequence (a ratio is taken less than 1.05) with increase of both $|x|$ and y.

Boundaries x_l and x_r are required to hold for the boundary conditions (13) and (14) performed with the following statements: (1) the hydrodynamic perturbation does not reach either boundaries, (2) the thermal perturbation does not reach the left boundary x_l, (3) the temperature gradient is equal to zero at the right boundary $x = x_r$. Our simulations showed that the locations of the left and right boundaries of the computational domain are strictly dependent on the Peclet number, and to satisfy the statements introduced above their absolute values increase as Pe decreases.

The water mass balance equation (7) together with Darcy's law given by (8) is discretized resulting in the following equation which may be treated as a discrete equation for pressure head $p_{ij} = p(x_i, y_j)$

$$(\Lambda_x + \Lambda_y)p = 0, \tag{17}$$

$$\Lambda_x p = \frac{1}{\hbar_i^x}\left(K^x_{i+0.5,j}\frac{p_{i,j} - p_{i+1,j}}{h_i^x} + K^x_{i-0.5,j}\frac{p_{i,j} - p_{i-1,j}}{h^x_{i-1}}\right),$$

$$\Lambda_y p = \frac{1}{\hbar_j^y}\left(K^y_{i,j+0.5}\frac{p_{i,j} - p_{i,j+1}}{h_j^y} + K^y_{i,j-0.5}\frac{p_{i,j} - p_{i,j-1}}{h^y_{j-1}}\right)$$

with harmonic mean representing hydraulic conductivity and liquid fluxes defined as

$$K^x_{i+0.5,j} = \frac{2k_{i,j}k_{i+1,j}}{k_{i,j} + k_{i+1,j}}, \quad K^y_{i,j+0.5} = \frac{2k_{i,j}k_{i,j+1}}{k_{i,j} + k_{i,j+1}},$$

$$k_{i,j} = K(S_{i,j}), \tag{18}$$

$$V^x_{i+0.5,j} = K^x_{i+0.5,j}\frac{p_{i,j} - p_{i+1,j}}{h_i^x},$$

$$V^y_{i,j+0.5} = K^y_{i,j+0.5}\frac{p_{i,j} - p_{i,j+1}}{h_j^y}. \tag{19}$$

The energy balance equation (10) is discretized in time using a fully implicit scheme for convective and conductive terms (an upwind scheme has been taken for convective term approximation)

$$\frac{T_{i,j} - \tilde{T}_{i,j}}{\tau} + \frac{St}{\tau}\left(S_{i,j} - \tilde{S}_{i,j}\right) + Pe(L_x + L_y)T + \Lambda T = 0, \tag{20}$$

$$\Lambda T = \frac{1}{\hbar_i^x}\left(\frac{T_{i,j} - T_{i+1,j}}{h_i^x} + \frac{T_{i,j} - T_{i-1,j}}{h^x_{i-1}}\right) + \frac{1}{\hbar_j^y}\left(\frac{T_{i,j} - T_{i,j+1}}{h_j^y} + \frac{T_{i,j} - T_{i,j-1}}{h^y_{j-1}}\right),$$

$$L_x T = \frac{1}{\hbar_i^x}\left(V^x_{i+0.5,j}T_{i,j} - V^x_{i-0.5,j}T_{i-1,j}\right),$$

$$L_y T = \frac{1}{\hbar_j^y}\left((V^y_{i,j+0.5})^+ T_{i,j} - (V^y_{i,j-0.5})^+ T_{i,j-1} + (V^y_{i,j+0.5})^- T_{i,j+1} - (V^y_{i,j-0.5})^- T_{i,j}\right).$$

Here, τ is the time step, *tilde* indicates values at the previous time level, while the other functions are taken at current time level, and superscripts $\pm$ denote the positive and/or negative part of the function. The upstream weighting used for the $L_x T$ term is written for the condition where $V^x > 0$ everywhere.

For the purpose of developing an algorithm that would be suitable for each type of zone, we reformulate the model and replace the function of concentration c by the function $\theta = Sc$ which represents an amount of solute accumulated in the pore voids. This transforms (11) to the following

$$S = S(T;\theta) = \begin{cases} 1 & \text{for } T \geqslant -\theta, \\ -\theta/T & \text{for } T \leqslant -\theta, \end{cases} \tag{21}$$

which gives a single-valued dependence of liquid water saturation on temperature. The reformulation forbids an existence of a pure solid zone ($S = 0$) because $S \to 0$ for $T \to -\infty$, and the mushy zone occurs for $T \leqslant -\theta$. If we further substitute θ in (9), it yields

$$\phi_t \frac{\partial\theta}{\partial t} + Pe\nabla\cdot\left(\frac{\theta}{S}\vec{V}\right) = 0.$$

One may see that the reformulation represents just a mathematical trick, which provides a suitable numerical method to attack a difficult non-linear problem.

Discretization of the balance equation for mass of solute gives

$$\frac{\phi_t}{\tau}\left(\theta_{i,j} - \tilde{\theta}_{i,j}\right) + Pe(L_x + L_y)\left(\frac{\theta}{S}\right) = 0, \tag{22}$$

where L_x and L_y are the operators defined above. It is known that discretization of the transport equation adopted in (22) results in numerical dispersion and, hence, a front smoothing. Fortunately, for the problem studied in this paper a front of concentration does not exist as solute is present everywhere initially.

The following iterative procedure is used to solve the system of non-linear discrete equations (17), (20)–(22) with four unknowns p, T, S, and θ. Each iterative sweep has the following steps:

(1) hydraulic conductivity is calculated by (18) using S determined from the previous iteration, and pressure head p is found by solving (17),
(2) liquid fluxes V_x and V_y are calculated by explicit formulae (19),
(3) solute content θ is calculated by solving (22),
(4) temperature T and saturation S are found by solving (20) and (21) simultaneously with V and θ defined at the previous iteration step.

For Step 1 the linear elliptic equation is solved by applying a high performance linear multigrid method [18,19]. Step 2 may be performed easily. In Step 3 to find θ we solve the linear equation (22) by a line Gauss–Seidel method moving along x and generating a tri-diagonal matrix for each column. The tri-diagonal matrix equation is solved using the Thomas algorithm [20]. Step 4 relates to the energy balance equation (20) containing the non-linear term $S(T)$ defined by (21). A fast convergence Newton–Raphson method [20,21] is invoked to solve (20) for temperature. This is expressed as

$$\frac{T_{i,j}-\tilde{T}_{i,j}}{\tau}+\frac{St}{\tau}\left(\widehat{S}_{i,j}-\tilde{S}_{i,j}+\left.\frac{\mathrm{d}\widehat{S}}{\mathrm{d}T}\right|_{i,j}\left(T_{i,j}-\widehat{T}_{i,j}\right)\right)+Pe(L_x+L_y)T+\Lambda T=0, \tag{23}$$

where *hat* indicates values at the previous iterative sweep. This scheme works very well if the function $S(T)$ is smooth. Unfortunately, the function

$$\frac{\mathrm{d}S}{\mathrm{d}T}(T;\theta)=\begin{cases}0 & \text{for } T>-\theta,\\ \theta/T^2 & \text{for } T<-\theta\end{cases}$$

has a discontinuity at $T=-\theta$. The value of $[\mathrm{d}S/\mathrm{d}T]=1/\theta$ at the discontinuity approaches infinity for a case of low initial concentration ($c_0\ll 1$). For such a case, saturation changes from zero to one within a very small zone treated as a freezing front. Iterating by the Newton–Raphson method causes an oscillation of the front position over its actual location. A combination of the Newton–Raphson method and any low-order iterative method is found to resolve this problem. We used a Gauss–Seidel method as a supplement to the Newton–Raphson method. One step of the combined scheme consists of a few (3–7) steps by Gauss–Seidel method followed by one step with the Newton–Raphson method. The algebraic non-linear equation

$$AT+BS(T)=F\quad(A>0,B>0)$$

arising at each step of the Gauss–Seidel method is solved explicitly by

$$T=\begin{cases}(F-B)/A & \text{for } F-B+A\theta\geqslant 0,\\ \left(F-\sqrt{F^2+4AB\theta}\right)/(2A) & \text{for } F-B+A\theta<0,\end{cases}$$

where the constants A, B, and F are determined by the values of temperature and saturation from the previous iterative sweep. This iterative procedure for solving (20) and (21) was found to have stable convergence for all simulations. A linear multigrid method is used to solve the linearized mesh problem given by (23).

4. Results and discussion

To verify the numerical model developed in Section 3, the solution should be compared with an appropriate analytical solution. The semi-analytical solution by Kornev and Mukhamadullina [6] which provides the equilibrium shape of the frozen region was used for this verification. The results of the comparison of the semi-analytical solution and the numerical solution are presented in Section 4.1. Following that verification, the analysis is extended in Section 4.2 to the case of freezing of aqueous solutions.

4.1. Freezing in the case of fresh water

The Stefan formulation characterized by the sharp interface separating solid and liquid regions is widely used for the study of fresh water freezing, i.e. $c_0=0$. For this situation, the steady-state semi-analytical solution [6] based on the complex variables technique gives an equilibrium shape of individual disjoined frozen bodies. The necessary condition for existence of this solution is given by the inequality

$$q<2Pe \tag{24}$$

We can confirm (24) by considering a heat balance over the whole domain at steady-state. Integrating (10) and using boundary conditions (13)–(16), it gives

$$q=2Pe(T_--T_+), \tag{25}$$

where $T_-=T(-\infty,y)=1$ is the input temperature at the left-hand side, while $T_+=T(\infty,y)=\text{constant}$ is the output temperature at the right-hand side. The temperature T_+ cannot be less than the freezing temperature of pure water (0 °C) if there is to be liquid flow at the right boundary at steady-state. Substituting the inequality $T_+>0$ into (25) we obtain that the freezing rate q should be less than $2Pe$, leading to (24). For the condition where $q>2Pe$ the individual frozen bodies eventually link up, thereby halting all liquid flow.

The procedure, introduced in Section 3, with minor modifications will be used for the numerical solution. For the case $c_0=0$, Step 3 in the numerical procedure is eliminated, and Eq. (11), as well as (21), is reduced to

$$S\in\mathscr{H}(T). \tag{26}$$

In numerical simulations we use Eq. (21) instead of (26), and assume that function θ is given by a constant very close to zero (10^{-5}–10^{-6}). This slightly smooths the discontinuity in S over $T=0$.

A uniform mesh with 64 nodes in the y direction and non-uniform mesh with 256 nodes in the x direction is used. The region $|x| < 1$ is covered by 128 nodes. We take the time-step τ being equal to about 10^5, representing a jump from the initial guess to the steady-state condition. A main iterative cycle containing steps 1–4 within the time step is stopped if the norm of residuals for Eqs. (17) and (20) becomes less than 10^{-5}. To reach convergence within a time step it usually required 7 or 8 main iterative cycles.

Numerical simulation results show that the domain $-\infty < x < \infty$, $0 \leqslant y \leqslant 1$ is divided into two subdomains. The first subdomain surrounds the freezing source $(x = 0, y = 0)$, and the function S is less than 10^{-5} at all nodes contained within the subdomain. This represents the solid region and may be treated as the frozen body. The other subdomain represents the liquid region where $S \equiv 1$. Transition from the solid to the liquid region is usually concentrated within two adjacent grid cells. The isotherm $T = 0$ is used to identify the freezing front.

Several steady-state frozen bodies are presented in Fig. 3 for $Pe = 5$. Solid lines numbered from 1 through 5 correspond to freeze rate $q = 5.208$, 7.2, 8.8, 9.5, and 9.95 respectively. For small q, the frozen body is almost a circle, and it increases infinitely along the liquid flow to the right as q approaches $2Pe$. The width of the frozen body at $x = \infty$ is demarcated by the dashed horizontal line for the limiting case $q = 2Pe$. The numerical results agree very well with the semi-analytical solution [6] (dotted lines in Fig. 3).

The time-dependent version of the numerical procedure is also applicable and will be used in the next section as a solution to the Stefan formulation to show the discrepancy with the solution for the general case $c_0 > 0$.

4.2. Freezing in the case of aqueous solutions

Eq. (9) for the balance of solute is involved in the numerical model when solute is present in the fluid. The presence of the solute will lead to the depression of the freezing temperature, thereby leading in general to a frozen body in which the saturation lies in the range $0 < S < 1$. In this section we are interested to address two aspects. The first is to evaluate whether the approximation by the Stefan formulation can adequately predict the outer shape of the frozen body in the case of an aqueous solution. This requires determining how much the frozen body shape obtained by solving the problem in the general formulation ($c_0 > 0$) is different from the one obtained by the Stefan formulation ($c_0 = 0$). The second aspect deals with the character of the frozen body development in the presence of solute. The numerical solution described in Section 3 will be used to address these two aspects. Two cases representing two distinct parameter sets will be employed for illustrative purposes.

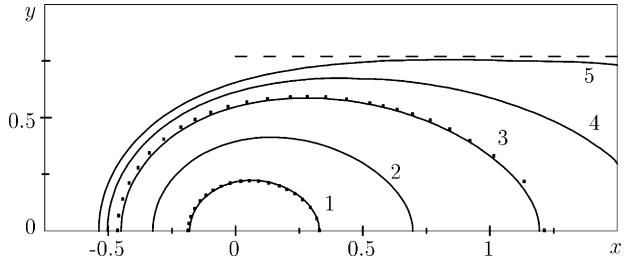

Fig. 3. Steady-state equilibrium shape of the frozen bodies for $Pe = 5$. The numbers from 1 to 5 correspond to the freeze rate $q = 5.208$, 7.2, 8.8, 9.5, and 9.95 respectively. Numerical solution is presented by solid lines, while the semi-analytical solution [6] is shown by dotted lines. The dashed horizontal line illustrates the width of the frozen body expanded infinitely far downstream from the freeze pipe for the limiting case $q = 2Pe$.

The first case considered is for a parameter set where $q > 2Pe$. The mesh used is the same as for the case of fresh water. The parameters for this case are: $c_0 = 0.5$, $Pe = 5$, $q = 30$, $St = 3$, and $\phi_t = 0.3$. The growth of the frozen body for this case is presented in Fig. 4 where the outer boundary of the frozen body is defined by the saturation isoline equal to 0.99. Isolines for saturations of 0.03, 0.1, 0.25, 0.5, 0.75, and 0.9 are shown by the solid lines, while the dashed line demarcates the interface obtained by the Stefan model ($c_0 = 0$). It is observed that the shape of the frozen body given by the Stefan model agrees well with the one obtained by the general model ($c_0 > 0$) in the part upgradient of the freeze pipes. The degree of agreement is somewhat less in the downgradient region. We found that this result held even for very high values of the initial concentration c_0.

Downgradient of the freeze pipe a wedge of saturated porous media develops. This occurs because the frozen region is only partially frozen and solute in the flow upgradient of the freeze pipe moves with the flow through the frozen body and concentrates due to freezing. The contribution of the flow through the frozen body to the total liquid flux is relatively small because the hydraulic conductivity decreases rapidly with decreasing saturation, e.g. $K(S) < 10^{-9}$ for $S < 10^{-3}$ and $n = 3$. Although the flow through the body is small, most of the flow entering the body does so in the vicinity of the point A as shown by the streamline plot in Fig. 5. As this flow passes through the body it is diverted downwards within the frozen body to exit downgradient of the freeze pipe near the x-axis. This causes the transport of an aqueous solution to the wedge region and accumulation of a relatively high concentrated liquid behind the freeze source, thereby delaying and even halting the growth of the frozen body there. Of course the Stefan approximation cannot account for this effect.

As mentioned before the frozen bodies will eventually link up for the case with $q > 2Pe$, and therefore there is no steady-state shape for the frozen body.

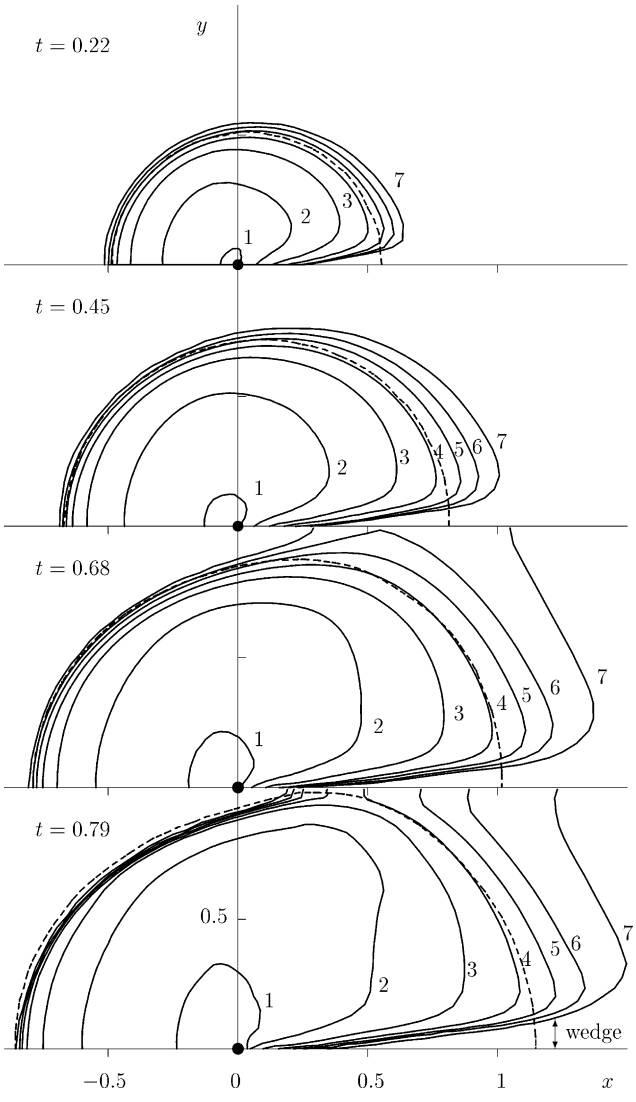

Fig. 4. Frozen body evolution and linking for the regime $q > 2Pe$ presented at different times for $q = 30$, $Pe = 5$ and $c_0 = 0.5$. The numbers from 1 to 7 correspond to degree of saturation $S = 0.03$, 0.1, 0.25, 0.5, 0.75, 0.9 and 0.99 respectively. The dashed line illustrates the interface obtained by the Stefan model ($c_0 = 0$).

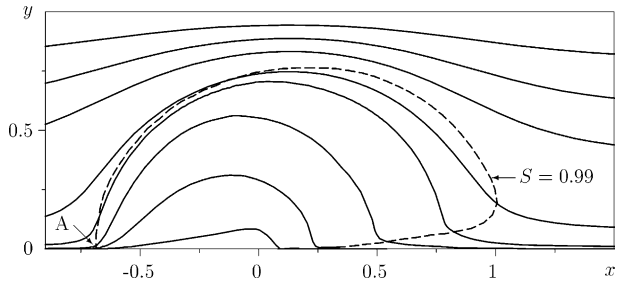

Fig. 5. Streamlines (—) and the shape of the frozen body (- - -) for the case presented in Fig. 4 at $t = 0.45$.

In the second case we consider the same set of parameters as in the first case except that we set q so that $q < 2Pe$. For this case there will be a steady-state shape to the frozen body as mentioned before. We used a non-uniform grid in both x and y directions with $h_j^y = 0.002$ within $0 \leqslant y \leqslant 0.05$.

A typical example of the evolution of the frozen body for the second case is presented in Fig. 6 for $c_0 = 0.5$, $Pe = 5$, $q = 6$, $St = 3$, and $\phi_t = 0.3$. The outer boundary of the frozen body is again represented by the saturation isoline equal to 0.99, and isolines for saturation are also shown. The solution provided by the Stefan model ($c_0 = 0$), which agrees very well with the outer boundary

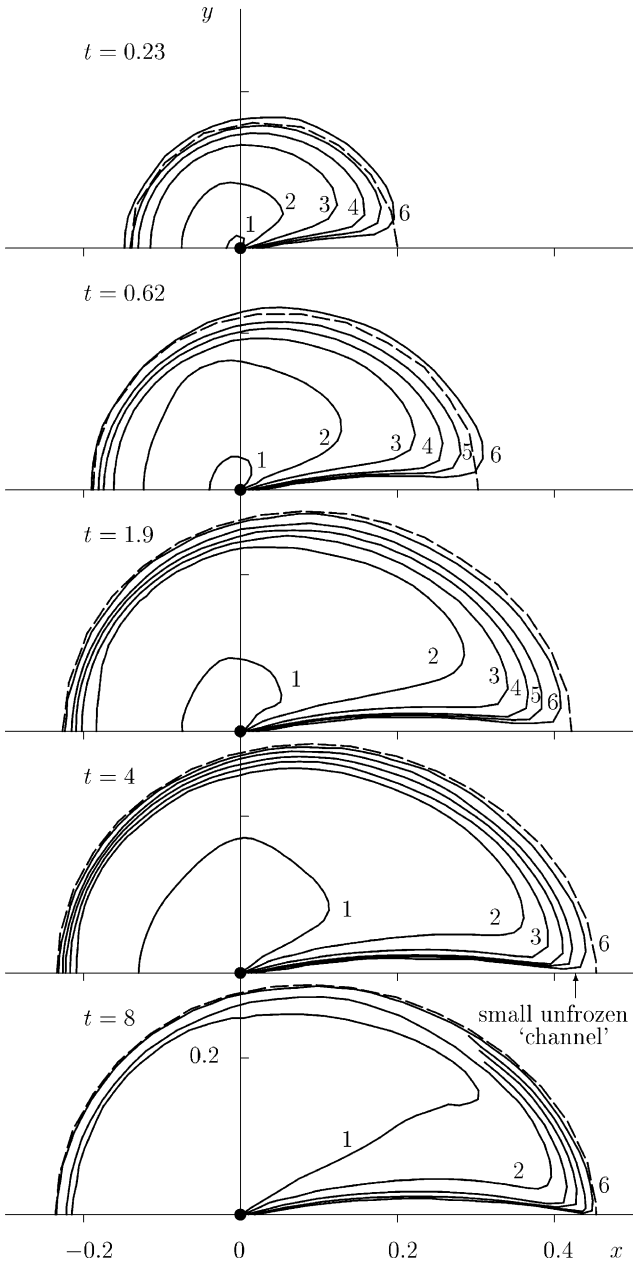

Fig. 6. Frozen body evolution and its equilibrium shape for the regime $q < 2Pe$ presented at different times for $q = 6$, $Pe = 5$ and $c_0 = 0.5$. The numbers from 1 to 6 correspond to degree of saturation $S = 0.03$, 0.1, 0.25, 0.5, 0.75 and 0.99 respectively. The shape of the frozen body for $c_0 = 0$ is shown by the dash line.

described by the general model, is presented by the dashed line.

The formation of a wedge of saturated porous media observed to occur for the first case is also seen to occur for this case as well, but in this case the behavior is distinctly different. In this case the downgradient ice-free zone is seen to first grow as a wedge shaped region, but after a time (at $t = 0.62$ for instance) the downgradient end of the wedge begins to grow toward the central axis of the flow. After a time ($t = 4$) the ice nearly grows to the central axis leaving only a very thin channel of ice-free porous media for the outflow of the liquid from the wedge. Eventually the frozen edge connects to the central axis forming a nearly parabolic liquid 'island'. The closure of the downgradient point will essentially cause cessation of flow out of the liquid island. The liquid in this liquid island cannot freeze because the solute concentration is sufficiently high to prevent further freezing and this becomes a permanent feature of the ice body because the liquid is trapped within the liquid island.

For these numerical solutions it was assumed that the molecular diffusion is zero, and therefore a gradient in the concentration of the solute within the liquid island exists once the flow out of the liquid island ceases. The concentration gradient is from the left to the right in the figure. If molecular diffusion had been assigned a finite non-zero value the solute concentration would equalize, and we hypothesize that this would keep the small channel open at the downgradient end and liquid would be able to escape. For that solution, the liquid island would shrink in size and eventually completely freeze.

The distribution of liquid saturation within the frozen body shown in Fig. 6 continues to develop such that eventually all saturation lines will collapse on the outside boundary, meaning that the body becomes fully frozen, and the shape of the body completely corresponds to the shape given by the Stefan model. This is also shown in Fig. 7 where the result for the steady-state Stefan model is demonstrated to coincide with the outside boundary simulated by the general solution. The case shown in Fig. 7 is for the same parameters in Fig. 6 except that the value of c_0 is 5.0. As for the case shown in Fig. 6, the saturation isolines within the frozen body will eventually collapse on the outside boundary. It is can be observed by comparison of the results in Figs. 6 and 7 that the width of the liquid island decreases with decrease in c_0.

We found that our numerical solution to the general formulation has a lower limit for the initial concentration equal to about $c_0 = 0.1$. For values of c_0 less than 0.1 the convergence of the numerical solution was found to be unsatisfactory. The problem with the convergence was identified to be associated with the formation of the liquid island. As mentioned previously, the width of the liquid island decreases with decrease in c_0. We hypothesize that as c_0 approaches zero the liquid island will degenerate into a bounded interval along the x axis. Such behavior poses difficulties for the numerical solution. We found that even with a very fine grid satisfactory convergence was not achieved. Solving this problem will require new numerical procedures.

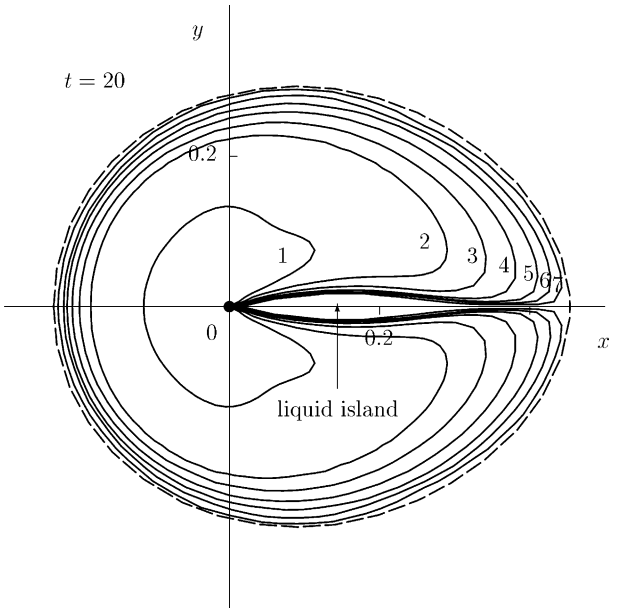

Fig. 7. Frozen body for $c_0 = 5$, $Pe = 5$ and $q = 6$ at $t = 20$. The numbers from 1 to 7 correspond to $S = 0.03$, 0.1, 0.25, 0.5, 0.75, 0.9 and 0.99, respectively. The equilibrium shape of the frozen body given by the Stefan model is presented by the dashed line.

5. Summary and conclusions

We have developed a numerical solution procedure to investigate the evolution of frozen bodies developed around freeze sources installed within flowing groundwater. The numerical solution for solving the coupled fluid flow, heat and solute transport equations with phase change is stable due to the use of an iterative scheme consisting of a combination of the Newton–Raphson method and the Gauss–Seidel method. The solution is applicable to the case of fresh water (the Stefan problem), as addressed by Kornev and Mukhamadullina [6], or to the general case of aqueous solutions. The unsteady process of frozen body evolution turns out to be different for the case of an aqueous solution in comparison to the case of fresh water. However, the frozen body boundary predicted by the Stefan solution was found to agree quite well with the outer boundary predicted by the general solution.

For the case of aqueous solutions, the frozen body is generally represented as a mushy zone, and the ability of liquid to move through it results in a zone of high concentrated brine downgradient of the freeze source.

Due to the high concentration, the zone cannot be frozen even after very large duration of freezing. For lower freezing rate this zone forms into a liquid 'island' that becomes a permanent feature of the frozen body. The width of the liquid island decreases with decrease in the initial solute concentration.

The numerical method was not able to handle the limiting case where the initial concentration approaches zero, because the liquid island becomes very thin, and this poses particular difficulties for the numerical solution. New numerical procedures will have to be developed to solve this problem.

Acknowledgements

Authors are very grateful to Prof. Rafail Dautov for discussions with regard to the developed numerical method, and to Prof. John Nieber for many helpful discussions leading to improvements of the manuscript. The first author would like to acknowledge a partial support provided by the Army High Performance Computing Research Center under the auspices of the Department of the Army, Army Research Laboratory cooperative agreement no. DAAD19-01-2-0014, the content of which does not necessarily reflect the position or the policy of the government, and no official endorsement should be inferred.

References

[1] Grant S, Iskandar IK. Artificially frozen ground as a subsurface barrier technology. In: Summary of workshop, Barrier technologies for environmental management. Washington: National Academy Press; 1997. p. D153–60.

[2] Moline GR. HRE-pond cryogenic barrier technology demonstration: Pre- and post-barrier hydrologic assessment, Technical Report 13701. Oak Ridge, TN: Oak Ridge National Laboratory; 1999.

[3] Goldstein ME, Reid RL. Effect of fluid flow on freezing and thawing of saturated porous media. Proc Royal Soc London Ser A 1978;364:45–73.

[4] Chugunov VA, Kornev KG. Dynamics of ice-rock barriers under conditions of freezing of filtering rocks. J Engng Phys 1986;51:981–6.

[5] Kornev KG, Chugunov VA. Determination of the equilibrium shape of the bodies formed during the solidification of filtration flow. J Appl Math Mech 1990;52:773–8.

[6] Kornev KG, Mukhamadullina GI. Mathematical theory of freezing for flow in porous media. Proc Royal Soc London Ser A 1994;447:281–97.

[7] Miller RD. Freezing phenomena in soils. New York: Academic Press; 1980. p. 254–99 [Chapter 11].

[8] O'Neill K. The physics of mathematical frost heave models: a review. Cold Reg Sci Technol 1983;6:275–91.

[9] Entov VM, Maksimov AM. Cooling of a salt solution. J Engng Phys 1986;51:1344–7.

[10] Panday S, Corapcioglu MY. Solute rejection in freezing soils. Water Resour Res 1991;27:99–108.

[11] O'Neill K, Miller RD. Exploration of a rigid-ice model of frost heave. Water Resour Res 1985;21:281–96.

[12] Honig JM. Thermodynamics: principles characterizing physical and chemical processes. In: Studies in modern thermodynamics, vol. 4. New York: Elsevier; 1982.

[13] Worster MG. Convection in mushy layers. Ann Rev Fluid Mech 1997;29:91–122.

[14] Chang CA, Chen F. Onset of plume convection in mushy layers. J Fluid Mech 2000;408:53–82.

[15] Luikov AV, Mikhailov YA. Theory of energy and mass transfer. Oxford: Pergamon Press; 1965.

[16] Egorov AG, Kosterin AV, Sheshukov A. One-dimensional problems of frozen soil thawing due to solution seepage. Fluid Dyn 1995;30:767–75.

[17] Sheshukov A, Egorov AG. Numerical modeling of coupled moisture, solute and heat transport in frozen soils. In: Lewkowicz AG, Allard M, editors. 7th International Conference on Permafrost, Université Laval, Yellowknife, Canada. 1998. p. 987–92.

[18] Hackbush W. Multigrid methods and applications. New York: Springer Verlag; 1985.

[19] Wesseling P. An introduction to multigrid methods. New York: Wiley; 1992.

[20] Press WH, Teukolsky SA, Vetterling WT, Flannery BP. Numerical recipes in C. Cambridge: Cambridge University Press; 1994.

[21] Samarskii AA, Nikolaev ES. Numerical methods for grid equations. Boston, MA: Birkhäuser Verlag; 1989.